Behavioral/Cognitive

Dopamine Modulates the Functional Organization of the Orbitofrontal Cortex

Thorsten Kahnt[1] and Philippe N. Tobler[2]

[1]Department of Neurology, Northwestern University Feinberg School of Medicine, Chicago, Illinois 60611, and [2]Department of Economics, Laboratory for Social and Neural Systems Research, University of Zürich, 8006 Zürich, Switzerland

Neuromodulators such as dopamine can alter the intrinsic firing properties of neurons and may thereby change the configuration of larger functional circuits. The primate orbitofrontal cortex (OFC) receives dopaminergic input from midbrain nuclei, but the role of dopamine in the OFC is still unclear. Here we tested the idea that dopaminergic activity changes the pattern of connectivity between the OFC and the rest of the brain and thereby reconfigures functional networks in the OFC. To this end, we combined double-blind, placebo-controlled pharmacology [D_2 receptor (D2R) antagonist amisulpride] in humans with resting-state functional magnetic resonance imaging and clustering methods. In the placebo group, we replicated previously observed parcellations of the OFC into two and six subregions based on connectivity patterns with the rest of the brain. Most importantly, while the twofold clustering did not differ significantly between groups, blocking D2Rs significantly changed the composition of the sixfold parcellation, suggesting a dopamine-dependent reconfiguration of functional OFC subregions. Moreover, multivariate decoding analyses revealed that amisulpride changed the whole-brain connectivity patterns of individual OFC subregions. In particular, D2R blockade shifted the balance of OFC connectivity from associative areas in the temporal and parietal lobe toward functional connectivity with the frontal cortex. In summary, our results suggest that dopamine alters the composition of functional OFC circuits, possibly indicating a broader role for neuromodulators in the dynamic reconfiguration of functional brain networks.

Key words: **connectivity; dopamine; fMRI; orbitofrontal cortex; parcellation**

Significance Statement

A key role of any neuromodulator may be the reconfiguration of functional brain circuits. Here we test this idea with regard to dopamine and the organization of functional networks in the orbitofrontal cortex (OFC). We show that blockade of dopamine D_2 receptors has profound effects on the functional connectivity patterns of the OFC, yielding altered connectivity-based subdivisions of this region. Our results suggest that dopamine changes the connectional configuration of the OFC, possibly leading to transitions between different operating modes that favor either sensory input or recurrent processing in the prefrontal cortex. More generally, our findings support a broader role for neuromodulators in the dynamic reconfiguration of functional brain networks and may have clinical implications for understanding the actions of antipsychotic agents.

Introduction

A key function of any neuromodulator may be to alter the dynamics and composition of functional brain circuits (Marder, 2012). By changing the intrinsic properties of neurons, neuromodulators can differentially affect the strength of individual synapses and may thereby bias neurons to transition between, and participate in, different functional circuits (Harris-Warrick and Marder, 1991; Weimann and Marder, 1994). Importantly, such network reconfigurations should be reflected in the functional connectivity profile of the brain regions hosting the functional circuit.

The orbitofrontal cortex (OFC) is one of the most connected regions of the brain and participates in several functional circuits (Kringelbach and Rolls, 2004; Zald and Rauch, 2008). It receives highly processed input from every sense, and is connected to other prefrontal areas, premotor cortex, and subcortical areas

Received Sept. 8, 2016; revised Nov. 18, 2016; accepted Dec. 28, 2016.

Author contributions: T.K. and P.N.T. designed research; T.K. performed research; T.K. analyzed data; T.K. and P.N.T. wrote the paper.

Research reported in this publication was supported by the National Institute on Deafness and Other Communication Disorders of the National Institutes of Health (NIH) under Award R01-DC-015426 (to T.K.), and by Swiss National Science Foundation Grants PP00P1_128574, PP00P1_150739, CRSII3_141965, and 00014_165884 (to P.N.T.). The content is solely the responsibility of the authors and does not necessarily represent the official views of the NIH. We thank H. Haker, T. Baumgartner, S. Weber, and M. Wälti for assistance in subject recruitment and data acquisition; and M. Mesulam, L.J. Chang, and J.D. Howard for helpful discussions, comments, and suggestions.

The authors declare no competing financial interests.

Correspondence should be addressed to Thorsten Kahnt, Northwestern University, Feinberg School of Medicine, Department of Neurology, 303 East Chicago Avenue, Ward 13-006, Chicago, IL 60611. E-mail: thorsten.kahnt@northwestern.edu.

DOI:10.1523/JNEUROSCI.2827-16.2016

 0270-6474/17/371493-12$15.00/0

such as the striatum, amygdala, hippocampus, and hypothalamus (Morecraft et al., 1992; Cavada et al., 2000). This dense connectome suggests that functional interactions with other brain regions are key to the processes that are performed by the OFC.

Important progress has been made in understanding how the OFC contributes to reward expectation, valuation, and decision-making (Sescousse et al., 2010; Padoa-Schioppa, 2011; Rushworth et al., 2012; Rudebeck and Murray, 2014; Howard et al., 2015; Stalnaker et al., 2015). However, although the frontal lobes receive strong projections from dopaminergic [dopamine (DA)] neurons in the midbrain (Swanson, 1982; Goldman-Rakic et al., 1992), and DA in the prefrontal cortex (PFC) has been associated with specific cognitive functions such as working memory and cognitive control (Miller and Cohen, 2001; Cools, 2016), characterizations of the role of DA in the OFC have remained relatively vague. Specifically, DA in the OFC has been linked to associative reward processing (Walker et al., 2009), reward-related instrumental behavior (Cetin et al., 2004), and, even more generally, to attention, motivation, and impulsive responding (Winstanley et al., 2010). Interestingly, systemic modulations of DA have been shown to alter long-range functional connections (Nagano-Saito et al., 2008; Cole et al., 2013a; Cole et al., 2013b), and DA in the OFC has been linked to dopaminergic neurotransmission in the striatum (Clarke et al., 2014), suggesting that DA may alter the functional connectivity between the OFC and remote brain regions.

Here we tested the idea that DA modulates the configuration of functional OFC networks. To this end, we combined DA pharmacology [using the specific D_2/D_3 receptor (D2R) antagonist amisulpride] with resting-state functional magnetic resonance imaging (fMRI) and connectivity-based clustering approaches. We parcellated the OFC into homogeneous subregions based on their functional connectivity patterns with the rest of the brain. In the placebo group, we replicated a previously observed parcellation into two and six subdivisions (Kahnt et al., 2012). Importantly, while the twofold clustering did not differ between groups, the sixfold parcellation differed significantly between groups, suggesting that blocking D2R reconfigured functional networks in the OFC. Moreover, multivariate decoding analyses revealed that whole-brain connectivity patterns of individual OFC subregions were modulated by amisulpride, such that functional connectivity with frontal cortex was enhanced, whereas connections with higher sensory areas were reduced by D2R blockade. These results suggest that monoamines play an important role for the composition of functional OFC circuits, possibly indicating a broader role of neuromodulators in the dynamic reconfiguration of functional brain networks.

Materials and Methods

Participants. A total of 78 healthy male subjects (mean ± SEM, 22.56 ± 0.27 years) participated in a resting-state fMRI session. Subjects received no visual stimulation and were asked to rest but to stay awake during the 6 min of scanning. One and one-half hours before the start of the resting-state scan (mean, 97.5 ± 0.35 min), subjects received either a pill containing placebo ($n = 53$) or 400 mg of the D2R blocker amisulpride ($n = 25$) in a double-blind, pseudorandomized fashion (ratio of placebo to amisulpride, 2:1). Groups did not differ significantly in age (placebo group, 22.62 ± 0.05 years; amisulpride group, 22.52 ± 0.08 years; $t_{(76)} = 0.18$, $p = 0.86$) and weight (placebo group, 75.06 ± 0.21 kg; amisulpride group, 75.08 ± 0.36 kg; $t_{(76)} = -0.01$, $p = 0.99$), and subjects were not aware of whether they received placebo or amisulpride, as assessed by a postexperimental questionnaire ($\chi^2 = 0.001$, $p = 0.99$). The study was approved by the Cantonal Ethics Review Board of Zurich, and subjects provided informed consent to participate.

fMRI acquisition. Functional imaging was performed on a Philips Achieva 3 T scanner equipped with an eight-channel head coil. A total of 180 T2*-weighted whole-brain echoplanar images with 37 transverse slices were acquired with a repetition time (TR) of 2000 ms. Imaging parameters were as follows: slice thickness, 3 mm; in-plane resolution, 2.75 × 2.75 mm; echo time (TE), 30 ms; flip angle, 90°. Temporal signal-to-noise ratio in the OFC did not differ between groups ($t_{(76)} = -1.07$, $p = 0.28$). For normalization purposes, a T1-weighted high-resolution (1 × 1 × 1 mm) structural image was acquired using the following imaging parameters: matrix size, 256 × 256; field of view, 256 × 256 mm; 181 slices; flip angle, 8°; TR, 8.2 ms; TE, 3.8 ms.

Preprocessing of fMRI images. Preprocessing of functional images was performed using SPM12 (Wellcome Department of Imaging Neuroscience, Institute of Neurology, London, UK) and consisted of slice-time correction, realignment, and coregistration of structural and functional images. Spatial normalization to the standard template of the Montreal Neurological Institute (MNI) was performed by estimating deformation fields based on the anatomical image. Deformation fields were used to write the following two sets of normalized functional images: one with a voxel size of 4 × 4 × 4 mm (4 mm set); and one with a voxel size of 3 × 3 × 3 mm (3 mm set). Both sets were spatially smoothed with a Gaussian kernel of 6 mm full-width at half-maximum.

Filtering of fMRI time series. Individual fMRI time series were filtered (Fox et al., 2009; Van Dijk et al., 2010) using a general linear model (GLM). The GLM contained the following: 1–6, six regressors related to between-scan head movements from the realignment procedure; 7, a constant term; 8, a linear trend; 9, the average signal from a white-matter mask; 10, the average signal from a CSF mask; and 11, the average signal from a gray-matter mask. The time series in each voxel was predicted using this set of 11 regressors, and the resulting residuals were high-pass filtered (cutoff, 128 s) and used for all subsequent analyses.

Orbitofrontal cortex and rest-of-brain mask. The OFC mask was defined using the following Automated Anatomical Labeling map labels: left and right superior orbital gyrus (2111, 2112); left and right middle orbital gyrus (2211, 2212); left and right inferior orbital gyrus (2321, 2322); left and right medial orbital gyrus (2611, 2612); and left and right rectal gyrus (2701, 2702). The resulting OFC mask combined voxels in the left and right medial and lateral orbitofrontal cortex. This OFC mask was subtracted from a whole-brain gray-matter mask, and the resulting voxels were defined as the rest-of-brain mask. Thus, there was no overlap between the rest-of-brain mask and the OFC mask.

Connectivity-based parcellation. We subdivided the OFC using a previously published method (Kahnt et al., 2012). In brief, for each OFC voxel, the time series correlation with every other voxel in the rest-of-brain mask was computed. The resulting connectivity vectors (one per OFC voxel) were then used to group together OFC voxels that have a similar connectivity profile with the rest of the brain. Similar methods have been used to subdivide brain regions using different measures of connectivity such as diffusion tractography (Johansen-Berg et al., 2004), resting-state fMRI (Kelly et al., 2010), and coactivations (Eickhoff et al., 2011).

We first computed the Pearson correlation coefficient between the time series in each OFC voxel (from the 3 mm set) and the time series in every other voxel in the rest-of-brain mask (from the 4 mm set) for each subject. Different voxel sizes were used to maintain high spatial resolution in the OFC while accommodating computational and memory limitations. This resulted in a 2-D correlation matrix ($N = 2771$ OFC voxels; $M = 12{,}724$ rest-of-brain voxels), where each row reflects the 1-by-M whole-brain connectivity pattern of one OFC voxel. Importantly, because voxels were in MNI space, each voxel has approximately the same anatomical position across subjects allowing averaging of connectivity matrices. Accordingly, individual matrices were averaged across subjects after transforming the correlation coefficients into Fisher's z-scores. The resulting N-by-M matrix was back-transformed into Pearson correlation coefficients and contained the average whole-brain connectivity patterns of all OFC voxels.

The parcellation was performed using the K-means clustering algorithm (*kmeans* as implemented in MATLAB, using the "correlation" option; i.e., one minus the correlation between the connectivity patterns

of OFC voxels as distance measure). Based on our previous study (Kahnt et al., 2012), we computed cluster solutions with $K = 2$ (K2) and $K = 6$ (K6) clusters. For each K, the parcellation was performed three times: once for the placebo group, once for the amisulpride group, and once for all subjects together (using a weighted average to account for the unequal group sizes). The parcellation was performed for all voxels in both hemispheres simultaneously. That is, for each K, the connectivity patterns from all OFC voxels were subjected to a single parcellation, regardless of the anatomical position (i.e., hemisphere) of a given voxel. For each K, we used the best solution from 100 repetitions with different initial centroids.

Note that the nominal labels assigned to the clusters are arbitrary and do not measure anything beyond cluster identity. To aid visual inspection and visual comparison between groupwise parcellations, and as a requirement for comparing the number of voxels per cluster between groups, the groupwise parcellations were relabeled to objectively match a template-labeling scheme taken from our previous study (Kahnt et al., 2012). For this, we permuted all $K!$ possible cluster label assignments and counted the number of voxels for which the cluster labels matched the template. We then relabeled the parcellation with the assignment that maximized this number. Voxelwise cluster maps in MNI space can be obtained from the corresponding author.

Between-group comparison of parcellations. We compared the parcellations between the placebo and amisulpride group using the variation of information (VI) metric (Meilă, 2007), which has previously been applied to fMRI connectivity-based parcellations (Kelly et al., 2010; Kahnt et al., 2012). The VI metric is based on mutual information and measures the distance between two cluster solutions (C and C'):

$$VI(C, C') = H(C) + H(C') - 2I(C, C'),$$

where $H(C)$ and $H(C')$ are the entropies of cluster solutions C and C', respectively, and $I(C, C')$ is the mutual information between C and C'. $H(C)$ and $I(C, C')$ are computed according to the following:

$$I(C, C') = \sum_{k=1}^{K}\sum_{k'=1}^{K'} P(k, k') \log\left(\frac{P(k, k')}{P(k)P(k')}\right)$$

$$H(C) = -\sum_{k=1}^{K} P(k) \log(P(k)),$$

where $P(k)$ is the probability that a voxel in cluster solution K belongs to cluster k and $P(k, k')$ is the probability that a voxel belongs to cluster k in C and cluster k' in C'. Following the definition by Meilă (2007), $P(k)$ and $P(k, k')$ are computed according to the following:

$$P(k) = \frac{N_k}{N}$$

$$P(k, k') = \frac{|C_k \cap C'_{k'}|}{N},$$

where N_k is the number of voxels in cluster k and N is the total number of OFC voxels. Low values of VI indicate high similarity between the two cluster solutions, whereas high VI values indicate large differences.

For statistical inference, we used a permutation test using the parcellations obtained from $n = 1000$ random group assignments. We compared the VI of the two empirical groupwise parcellations with the distribution of the VI of pairs of parcellations obtained from randomly assigned groups. For each permutation, we randomly assigned subjects to two groups (keeping the original group sizes), computed the groupwise parcellations for these new groups, and computed the VI between the two parcellations. The empirically observed VI was considered significant if larger VI values were found in <5% of the 1000 random parcellation pairs ($p < 0.05$).

Hemispheric symmetry. To quantify the hemispheric symmetry of the obtained parcellations, we computed a symmetry index (SI; Kahnt et al., 2012). This measure reflects the overlap in cluster labels between hemispheres, if one hemisphere is mirrored at the midline, as follows:

$$\mathrm{SI} = \frac{1}{N}\sum_{i}^{N}\begin{cases} 1 \text{ if } x_i = x'_i \\ 0 \text{ otherwise} \end{cases}$$

where N is the number of voxels in one hemisphere and x and x' are the cluster labels of voxel i in the original and mirrored parcellation, respectively. Because this measure requires that each voxel exists in both hemispheres, we included only voxels that are present in both hemispheres and discarded all voxels that are present on one side only. Differences in hemispheric symmetry were compared between groups, and statistical inference was performed using a permutation test with $n = 1000$ random group assignments (see Between-group comparison of parcellations).

Connectivity-based decoding of drug condition. To test whether D2R blockade altered the functional connectivity profile of OFC subregions, we used a between-subject multivariate decoding approach. We aimed to decode the drug condition (amisulpride vs placebo) based on the whole-brain connectivity patterns of individual OFC subregions in the K2 and K6 parcellations. To avoid biases, we used the K2 and K6 parcellations computed from all subjects. In contrast to conventional multivoxel pattern analysis approaches that use multivoxel patterns of activity, here we used multivoxel patterns of functional connectivity of individual OFC subregions. For each subject, we computed the functional connectivity (Pearson correlation) between the time series in each OFC subregion (averaged across voxels) and every other voxel in the rest-of-brain mask, resulting in two and six 1-by-M connectivity patterns, for K2 and K6, respectively. For each k in K, the subjectwise 1-by-M connectivity patterns were mean normalized across voxels (resulting in zero-mean vectors) and used as feature vectors in a support vector machine (SVM) classifier (http://www.csie.ntu.edu.tw/~cjlin/libsvm/) with a linear kernel, and 500 random leave-two-subjects-out cross-validation steps. For each cross-validation step, we randomly drew 25 subjects from each group for obtaining training data, and from this subset randomly left out 1 subject per group for use as the test data. We then used the training data (excluding the two left-out test subjects) to train the SVM to distinguish between subjects from the two groups, based on the whole-brain connectivity pattern of the kth OFC subregion. The classifier was then tested on the two subjects who were left out, and the procedure was repeated for the next cross-validation step. Decoding accuracy (i.e., the percentage correct classification in the test data) was averaged across the 500 cross-validation steps.

For statistical inference, we performed a permutation test ($n = 1000$), in which we compared the empirical decoding accuracy to the distribution of decoding accuracies resulting from random permutations of group labels. Specifically, we repeated the identical 500-step cross-validation procedure described above with the exception that after randomly drawing 25 subjects and assigning 2 subjects for obtaining test data, we randomly shuffled the group labels in the training and the test data. This was repeated 1000 times to generate a distribution of accuracies. The empirically observed decoding accuracy was considered significant if larger decoding accuracies were found in <5% of the 1000 random permutations ($p < 0.05$).

Mapping of informative voxels. To illustrate the rest-of-brain voxels for which functional connections with OFC subregions were modulated by DA, we examined the weight vector of the SVM classifier. However, rather than directly using the weight vectors from the SVM decoding (i.e., backward) model, we first constructed an encoding (i.e., forward) model based on these weights according to the definition by Haufe et al. (2014) as follows:

$$A = S_x W S_g^{-1},$$

where W is the weight vector of the SVM decoder, and S_x and S_g are the covariance matrices of the training features and labels, respectively.

In contrast to the weights of backward models, the weights of forward models can be interpreted as reflecting the contribution of individual voxels to the separation between the two groups. We averaged the voxelwise forward weights across the 500 cross-validation steps and divided each weight average by the corresponding SD. This resulted in z-scores that, for a given OFC subregion, reflect the contribution of voxelwise connectivity to the separation between groups. We report connections

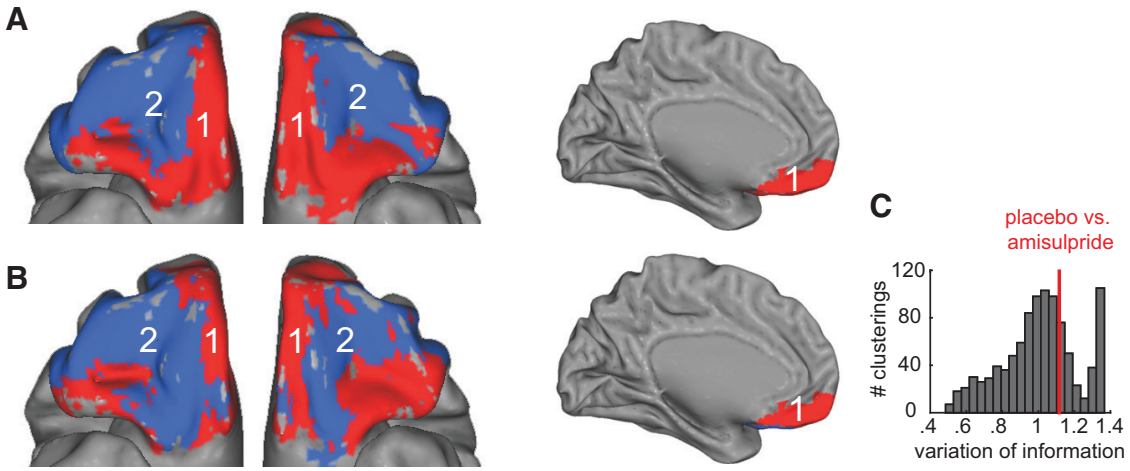

Figure 1. Connectivity-based parcellation of the OFC into K2 subregions. ***A***, Twofold clustering in the placebo group. ***B***, Twofold clustering in the amisulpride group. ***C***, Histogram of *VI* values comparing pairs of K2 parcellations from random group assignments. Red vertical line depicts the *VI* value comparing the actual groupwise parcellations of the placebo and amisulpride group.

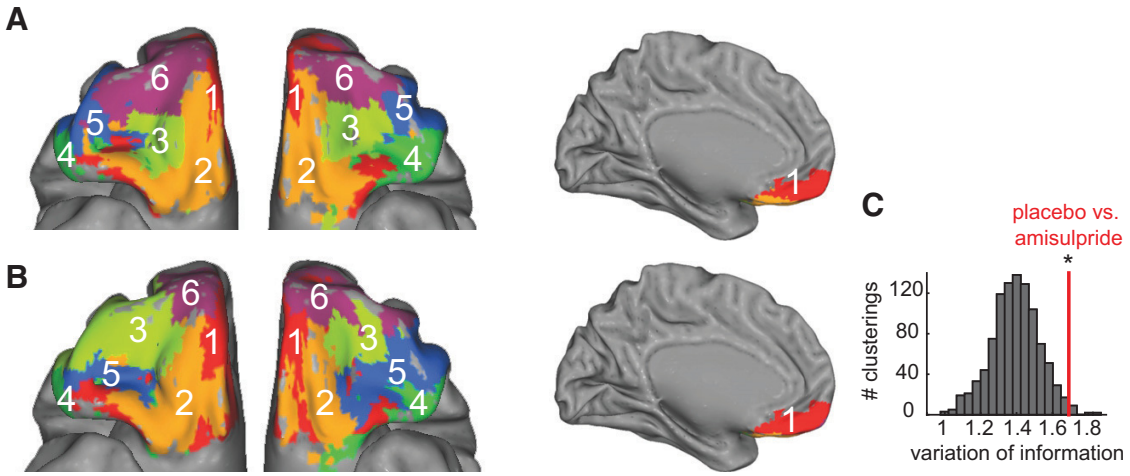

Figure 2. Connectivity-based parcellation of the OFC into K6 subregions. ***A***, Sixfold clustering in the placebo group. ***B***, Sixfold clustering in the amisulpride group. ***C***, Histogram of *VI* values comparing pairs of K6 parcellations from random group assignments. Red vertical line depicts the *VI* value comparing the actual groupwise parcellations of the placebo and amisulpride groups. Asterisk indicates a significant group difference from chance at $p < 0.05$.

that exceed a threshold of $p < 0.05$, Bonferroni corrected for the number of rest-of-brain voxels ($z > 4.47$) and that exceed a cluster extent of 2 voxels. For illustration purposes, we display the connectivity maps at a threshold of $p < 0.001$, uncorrected ($z > 3.72$) with a cluster size of >5 voxels.

Results

Connectivity-based parcellation of the OFC

Based on our previous findings (Kahnt et al., 2012), we subdivided the OFC into K2 and K6 subregions by grouping together voxels that have a similar pattern of connectivity with the rest of the brain. In a first step, we focused on the placebo group to reveal the functional organization when neuromodulatory activity is undisturbed. The K2 parcellation separated each hemisphere into (1) a medial subregion and (2) an anterior lateral subregion (Fig. 1*A*). The ventromedial wall (areas 14m and 10; Mackey and Petrides, 2010), the gyrus rectus (areas 11m, 14r, and 14c), posterior (area 13), and posterior lateral (area 47/12o) areas formed a network, whereas the remainder of the OFC, that is, central area (11), anterior area (10), and anterior lateral area (47/12m) formed another network with cohesive connectivity patterns.

In line with our previous findings (Kahnt et al., 2012), the K6 parcellation revealed (1) a medial, (2) a posterior-medial, (3) a central, and three (4–6) lateral clusters spanning the anterior-posterior gradient (Fig. 2*A*). In terms of cytoarchitecture, the medial cluster occupied most of the ventromedial wall (areas 14m, 10, and 11m) in addition to a small focal part of the lateral posterior OFC (area 13). The posterior–medial cluster consisted of large parts of the gyrus rectus (areas 11m, 14r, 14c), as well as parts of more lateral posterior (area 13) areas. Regions at the intersection of the transverse and medial orbital sulcus (area 11) formed a central cluster. Finally, the three lateral clusters occupied the posterior-lateral area (47/12o), midlateral area (47/12m), and anterior-lateral area (10, 11) surface. Overall, both the K2 and K6 parcellations in the placebo group were highly similar to our previous findings (Kahnt et al., 2012).

Dopamine changes the connectivity-based parcellation of the OFC

We next examined how altering dopaminergic neurotransmission through D2R blockade modulated the connectivity-based parcellations described above. Similar to the placebo group, the K2 solution in the amisulpride group revealed (1) a medial cluster and (2) an anterior-lateral cluster (Fig. 1*B*). Compared

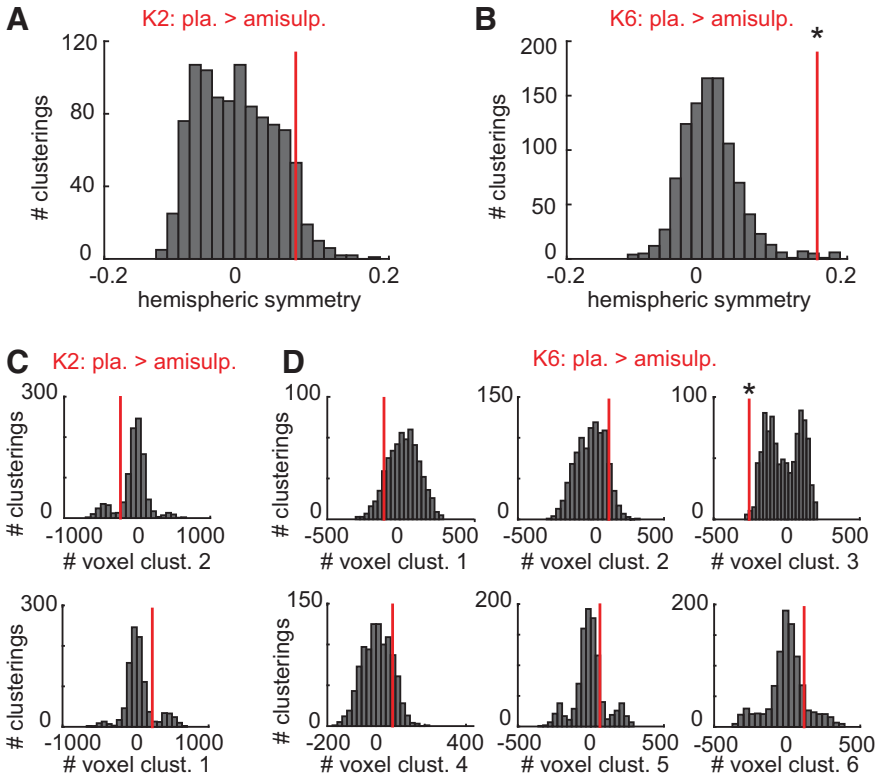

Figure 3. Comparison of groupwise parcellations. ***A***, Histogram of the difference in hemispheric symmetry between the pairs of K2 parcellations from randomly assigned groups. Red vertical line depicts the empirical difference in hemispheric symmetry between the placebo group and the amisulpride group. ***B***, Same as in ***A***, but for the K6 parcellation. ***C***, Each histogram depicts the difference in the cluster size (number of voxels) between two randomly assigned groups in clusters 1 (top) and 2 (bottom) of the K2 parcellation. Red vertical lines depict the empirical difference in cluster size between the placebo and amisulpride groups. ***D***, Same as in ***C***, but for the K6 parcellation. Asterisks indicate significant differences from zero at $p < 0.05$.

with the placebo group, the anterior-lateral cluster appeared narrower and more stretched along the anterior–posterior axis, dividing the medial cluster into a medial and posterior-lateral segment. However, despite these qualitative differences, a quantitative statistical comparison of the parcellations between the two groups using the *VI* metric revealed that the differences in the K2 parcellation are within the range of what can be expected by chance ($p = 0.278$; Fig. 1*C*). In line with this, there were no significant differences between groups in hemispheric symmetry (placebo, $SI = 0.93$; amisulpride, $SI = 0.84$; $p = 0.08$, permutation test; Fig. 3*A*), or cluster sizes ($p = 0.169$; Fig. 3*C*). These findings may indicate that the two-cluster organization of the OFC was not substantially altered by changes in dopaminergic neurotransmission.

In contrast, D2R blockade appeared to have caused more pronounced changes in the K6 parcellation (Fig. 2*B*). Indeed, a permutation test using the *VI* metric revealed that the K6 parcellations were significantly different between the two groups ($p = 0.013$; Fig. 2*C*). Qualitatively, while the medial cluster (1) and posterior-medial cluster (2) appeared relatively similar to the placebo group, no clearly defined central cluster (3) could be observed in the amisulpride group. Instead, a fourth cluster was revealed on the lateral surface between the anterior lateral and mid-lateral clusters. In line with this, the number of voxels assigned to the central cluster (3) was significantly larger in the amisulpride group compared with the placebo group (amisulpride, $N = 491$; placebo, $N = 234$; $p = 0.004$; Fig. 3*D*), while the size of the other clusters did not differ significantly (all $p > 0.235$). In addition, the hemispheric symmetry was significantly larger in the placebo group (placebo group, $SI = 0.87$; amisulpride group, $SI = 0.69$; $p = 0.009$; Fig. 3*B*), suggesting that D2R blockade disturbed the symmetry of the functional OFC networks. Together, these results demonstrate that the connectivity-based parcellation of the OFC was changed by D2R blockade, suggesting that DA reconfigures functional OFC networks.

Dopamine alters connectivity patterns of individual OFC subregions

The results reported above suggest that the functional connectivity between individual OFC voxels and the rest of the brain was systematically altered by D2R blockade, indicating a DA-dependent reconfiguration of functional OFC networks. In principle, DA-induced changes in the functional connectivity of the OFC could be localized to specific parts of the brain, or could involve the simultaneous modulation of distributed long-range connections. To directly test for such changes in the connectivity patterns of OFC subregions, we used a multivariate decoding approach. Specifically, for each subregion in the K2 and K6 parcellation, we used its whole-brain connectivity pattern to decode whether subjects had received placebo or amisulpride before scanning. To avoid biases, we used a parcellation that was based on all subjects (Fig. 4*A*,*B*; however, comparable results were obtained when using the parcellation based on the placebo group only).

Decoding of group membership from the whole-brain connectivity patterns of both clusters in the K2 parcellation was significantly above chance [medial cluster (1): accuracy = 58.5%, $p < 0.001$; anterior lateral cluster (2): accuracy = 55.2%, $p = 0.001$; Fig. 4*C*]. In the K6 parcellation, we found that drug condition could be decoded significantly above chance from the connectivity patterns of all but two OFC subregions. Significant decoding accuracies were found in the medial cluster (1, accuracy = 54.8%, $p = 0.001$), posterior-medial cluster (2, accuracy = 60.2%, $p < 0.001$), central cluster (3, accuracy = 60.0%, $p < 0.001$), and anterior-lateral cluster (6, accuracy = 57.6%, $p < 0.001$). The decoding accuracies in the posterior-lateral cluster (4, accuracy = 50.4%, $p = 0.415$) and mid-lateral cluster (5, accuracy = 51.7%, $p = 0.145$) were not significantly different from chance. In summary, D2R blockade modulated the whole-brain connectivity patterns of medial and central OFC sectors, while leaving the connectivity of the posterior-lateral clusters unaffected.

To reveal the brain regions in which the connectivity to individual OFC subregions was modulated by D2R blockade, we used the weights of the SVM classifier to estimate voxelwise connectivity patterns that distinguished between groups (Haufe et al., 2014). For the K2 parcellation, D2R blockade enhanced the connectivity of the medial OFC cluster (1) with the amygdala/hippocampus, the superior frontal gyrus, the anterior cingulate cortex, the posterior insula, and the anterior inferior and middle

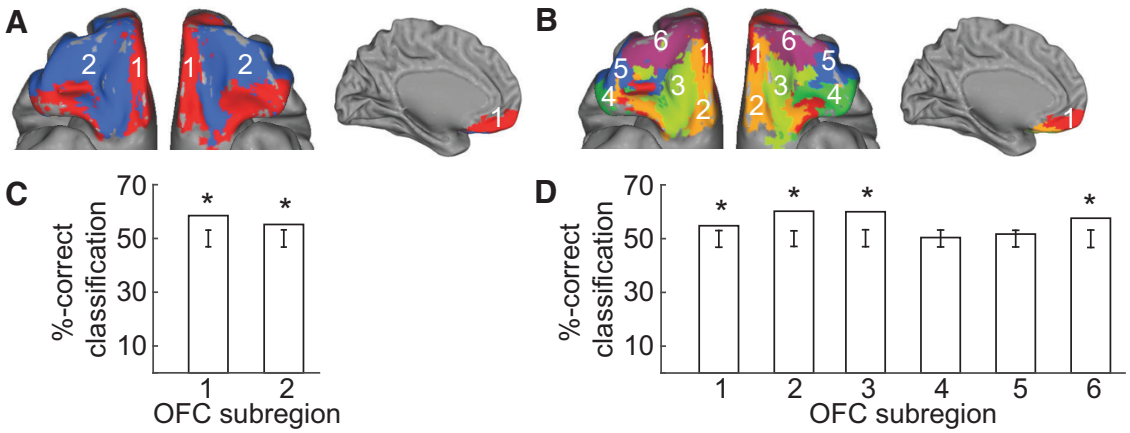

Figure 4. Decoding drug condition from connectivity patterns of individual OFC subregions. ***A***, K2 parcellation based on all subjects. ***B***, K6 parcellation based on all subjects. ***C***, Decoding accuracy (percentage correct group classifications of placebo vs amisulpride) for each of the two OFC subregions of the K2 parcellation. ***D***, Decoding the accuracy for each of the six OFC subregions of the K6 parcellation. Error bars indicate 95% confidence intervals around the level of empirical chance (~50%) based on 1000 random permutations. Asterisks indicate significant above-chance classification at $p < 0.05$, corrected.

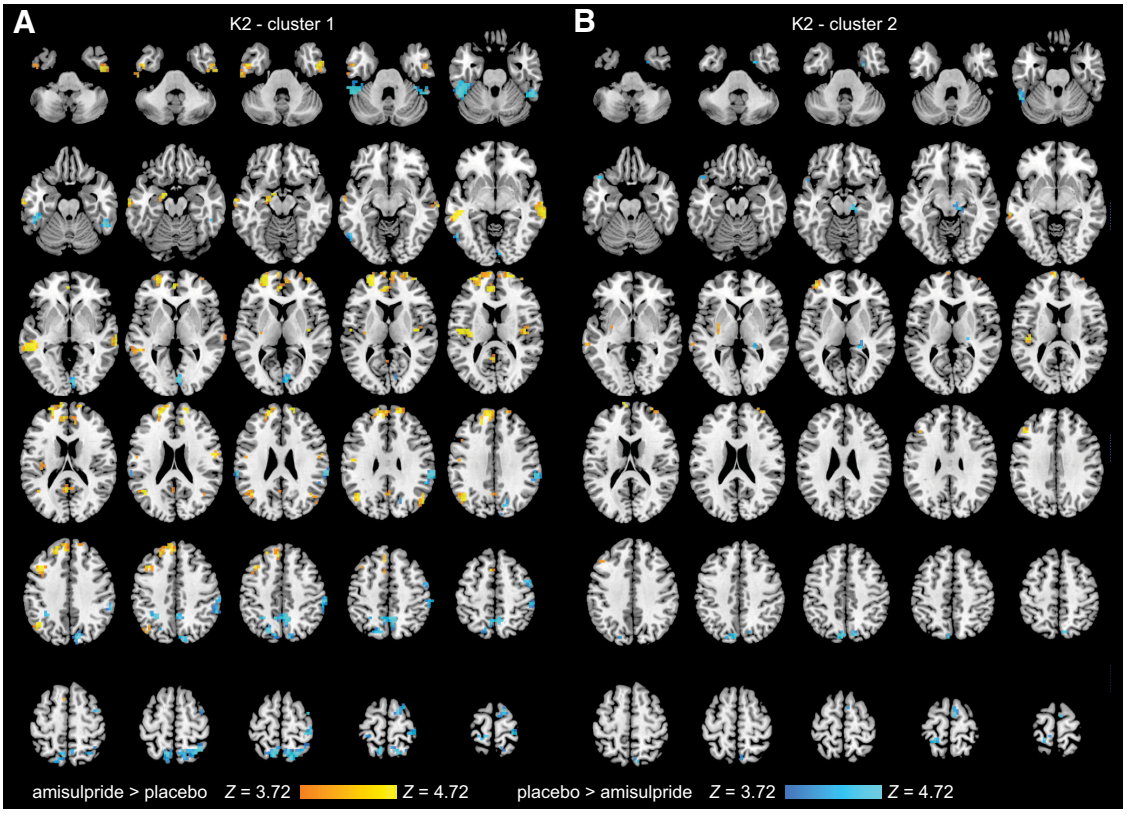

Figure 5. Effects of D2R blockade on voxelwise OFC connectivity of K2 subregions. ***A***, ***B***, Maps depict the contribution of the voxelwise connectivity of the medial (***A***) and lateral (***B***) OFC subregion of the K2 parcellation to the separation between the amisulpride and placebo groups. Connectivity patterns are estimated based on SVM weight vectors and then converted into *z*-scores. For illustration purposes, maps are thresholded at $p < 0.001$, uncorrected ($z > 3.72$) with a voxel extent threshold of 5.

temporal gyrus (Fig. 5*A*, Table 1). Conversely, amisulpride reduced the connectivity of the medial OFC cluster with posterior inferior temporal gyrus, fusiform gyrus, precuneus, and inferior and superior parietal lobes. In the anterior-lateral cluster (2), D2R blockade enhanced connectivity with the medial and middle frontal gyri and the posterior insula, and reduced connectivity with the midbrain, the fusiform gyrus, the precuneus, and the superior parietal lobe (Fig. 5*B*, Table 1).

In the K6 parcellation, D2R blockade enhanced connectivity between the medial OFC cluster (1) and the superior and middle frontal gyri, the anterior cingulate cortex, and the inferior and middle temporal gyri. In contrast, subjects in the amisulpride group showed reduced medial OFC connectivity with the fusiform gyrus and superior parietal lobe (Fig. 6*A*, Table 2). In turn, D2R blockade enhanced connectivity of the posterior-medial OFC cluster (2) with the left amygdala/hippocampus and the middle frontal gyrus, while connectivity with the anterior insula and the precuneus was reduced (Fig. 6*B*, Table 2). For the central cluster (3), D2R blockade enhanced connectivity with the middle temporal lobe and the fusiform gyrus. However, the most pro-

Table 1. Dopamine-dependent connectivity of subregions in the K2 parcellation

Side	Anatomical label	MNI coordinates			*N* voxel	*z*-score
		x	*y*	*z*		
Cluster 1: amisulpride > placebo						
L	Amygdala/hippocampus	−14	−4	−18	5	6.09
L	Superior frontal gyrus	−26	56	6	49	6.99
R	Superior frontal gyrus	26	68	10	16	5.29
L	Anterior cingulate cortex	−6	48	14	14	6.69
L	Superior frontal gyrus	−18	44	38	4	5.99
L	Middle frontal gyrus	−42	44	38	6	5.02
L	Insula	−38	−16	14	12	5.43
R	Insula	38	−12	10	5	6.09
L	Middle temporal gyrus	−54	−36	−6	22	5.51
R	Middle temporal gyrus	70	−32	−6	12	5.45
L	Middle temporal gyrus	−66	−16	−22	3	5.33
L	Inferior temporal cortex	−50	−4	−34	3	4.83
R	Inferior temporal cortex	54	−4	−34	3	5.56
L	Precuneus	−2	−52	18	3	5.03
L	Inferior parietal lobe	−42	−64	34	17	5.70
Cluster 1: placebo > amisulpride						
R	Middle frontal gyrus	42	0	58	3	4.61
R	Superior frontal gyrus	14	0	70	3	5.14
R	Precentral gyrus	38	−32	66	3	5.48
L	Postcentral gyrus	−10	−36	78	5	5.67
L	Middle temporal gyrus	−54	−64	−6	3	4.98
L	Fusiform gyrus	−50	−44	−26	33	7.17
R	Fusiform gyrus	50	−44	−30	14	6.27
L	Precuneus	−10	−52	46	36	6.65
R	Precuneus	6	−52	46		6.48
R	Superior parietal lobe	18	−60	66	21	5.34
L	Inferior parietal lobe	−26	−52	42	6	5.96
R	Inferior parietal lobe	66	−32	30	15	6.21
R	Occipital cortex	2	−84	2	8	5.07
Cluster 3: amisulpride > placebo						
L	Medial frontal gyrus	−6	68	14	4	5.43
L	Middle frontal gyrus	−42	28	34	3	4.69
L	Insula	−46	−24	14	3	4.77
Cluster 2: placebo > amisulpride						
R	Midbrain	14	−24	−14	4	6.76
L	Fusiform gyrus	−50	−52	−26	3	4.93
L	Precuneus	−6	−80	46	10	5.76
L	Superior parietal lobe	−18	−40	74	3	5.02

Anatomical labels, MNI coordinates (*x*, *y*, *z*), *z*-scores, and cluster size (number of voxels) for whole-brain connectivity of individual OFC subregions in the K2 parcellation contributing to the separation between groups, thresholded at $p < 0.05$, Bonferroni corrected ($z > 4.47$) and $k > 2$. L, Left; R, right.

found change was a marked reduction in connectivity to the midbrain and the superior temporal gyrus/posterior insula (Fig. 6*C*, Table 2). Finally, for the anterior-lateral OFC cluster (6), D2R blockade enhanced connectivity with lateral and medial areas of the PFC, the anterior cingulate cortex, and the middle temporal gyrus. In contrast, amisulpride reduced connectivity of the anterior-lateral OFC with the entorhinal cortex, the posterior hippocampus, and the precuneus (Fig. 6*D*, Table 2). We did not examine dopamine-dependent modulation of connectivity in the posterior-lateral (4) and mid-lateral (5) OFC clusters because the decoding analyses reported above indicated that the connectivity patterns of these OFC subregions were not significantly modulated by D2R blockade.

Discussion

In the current study, we used resting-state fMRI connectivity and *K*-means clustering, and demonstrated that the systemic administration of amisulpride, a dopaminergic D2R antagonist, altered the configuration of connectional and presumably functional subregions in the OFC. Moreover, D2R blockade had specific effects on voxelwise connectivity patterns of individual OFC subregions, as indicated by significant decoding of group membership (amisulpride vs placebo) from these patterns. Amisulpride decreased the connectivity between OFC and associative parietal and temporal regions, and enhanced the connectivity of OFC subregions with the medial and superior-lateral frontal cortex.

Previous studies have examined the effects of dopaminergic neurotransmission on large-scale fMRI connectivity during rest (Cole et al., 2013a,b) and task performance (Honey et al., 2003; Nagano-Saito et al., 2008). The results of these earlier studies indicate that DA has profound effects on long-range connectivity among frontal, parietal, and subcortical brain regions. However, these studies compared connectivity within predefined regions of interest or "resting-state networks" (e.g., the so-called "default mode" network) and were therefore not suitable to examine the effects of DA on the configuration of functional circuits themselves.

In contrast, here we used a data-driven method to define functional OFC subregions based on whole-brain connectivity patterns of individual OFC voxels. Based on our earlier study (Kahnt et al., 2012), anatomical tracing work in primates (Carmichael and Price, 1996; Ongür and Price, 2000), and the results of a meta-analytic connectivity modeling study (Zald et al., 2014), we focused on the parcellations with 2 and 6 subdivisions. The par-

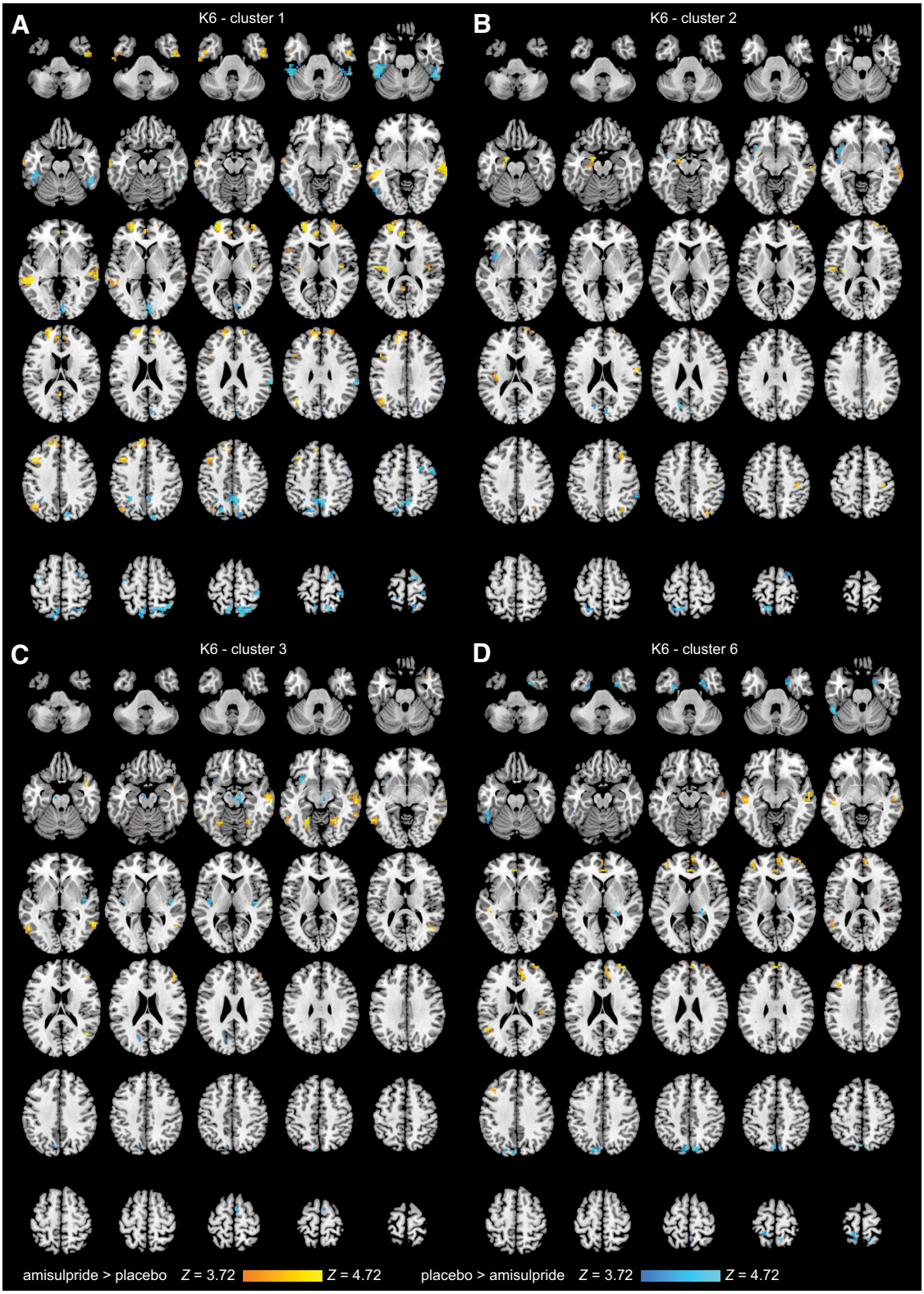

Figure 6. Effects of D2R blockade on voxelwise OFC connectivity of K6 subregions. ***A–D***, Maps depict the contribution of the voxelwise connectivity of the medial (***A***), posterior-medial (***B***), central (***C***), and anterior-lateral (***D***) OFC subregions of the K6 parcellation to the separation between the amisulpride and placebo groups. Connectivity patterns are estimated based on SVM weight vectors and then converted into *z*-scores. For illustration purposes, maps are thresholded at $p < 0.001$, uncorrected ($z > 3.72$) with a voxel extent threshold of 5.

cellations obtained in the placebo group were highly similar to those found in our previous study (Kahnt et al., 2012), whereas the parcellation in the amisulpride group revealed specific changes in the organization of functional OFC subregions. Specifically, whereas the K2 parcellation did not differ between groups, the organization of the K6 parcellation differed fundamentally, particularly with regard to the central OFC cluster. Follow-up analyses indicated that D2R blockade was associated

Table 2. Dopamine-dependent connectivity of subregions in the K6 parcellation

		MNI coordinates				
Side	Region	*x*	*y*	*z*	*N* voxel	*z*-score
Cluster 1: amisulpride > placebo						
L	Superior frontal gyrus	−26	56	6	42	7.84
L	Superior frontal gyrus	−6	52	30	4	5.23
L	Superior frontal gyrus	−18	44	38	5	5.16
R	Superior frontal gyrus	18	56	26	4	5.11
L	Middle frontal gyrus	−42	16	38	10	5.52
L	Anterior cingulate cortex	−6	48	14	8	6.67
L	Insula	−38	−16	14	8	5.29
R	Insula	38	−12	10	3	5.84
L	Middle temporal gyrus	−46	−28	−6	22	6.07
R	Middle temporal gyrus	66	−28	−2	22	5.34
L	Inferior temporal gyrus	−58	−16	−34	3	4.90
R	Inferior temporal gyrus	46	−12	−42	14	6.16
L	Inferior parietal lobe	−46	−64	38	8	5.13
Cluster 1: placebo > amisulpride						
R	Superior frontal gyrus	14	−4	70	3	5.14
R	Middle frontal gyrus	46	0	54	3	4.91
L	Postcentral gyrus	−10	−40	78	3	4.90
R	Postcentral gyrus	38	−32	66	6	5.68
L	Inferior temporal gyrus	−50	−40	−26	31	6.94
R	Inferior temporal gyrus	50	−48	−26	16	5.75
L	Inferior temporal gyrus	−54	−60	−6	3	4.66
R	Superior parietal gyrus	18	−60	66	23	6.31
R	Precuneus	6	−52	46	28	6.26
L	Precuneus	−14	−68	50	4	5.19
L	Inferior parietal lobe	−26	−52	42	3	5.29
R	Inferior parietal lobe	66	−28	26	5	5.20
R	Occipital cortex	6	−80	2	4	4.61
Cluster 2: amisulpride > placebo						
L	Amygdala/hippocampus	−18	−4	−18	8	6.32
R	Middle frontal gyrus	38	60	14	3	5.12
R	Postcentral gyrus	38	−24	50	3	5.22
Cluster 2: placebo > amisulpride						
L	Insula	−38	12	−6	3	4.69
L	Middle frontal gyrus	−38	0	54	3	4.73
R	Superior temporal gyrus	46	−12	−2	3	5.55
L	Precuneus	−22	−56	66	7	4.96
L	Precuneus	−18	−68	26	3	5.82
Cluster 3: amisulpride > placebo						
R	Middle temporal gyrus	58	−12	−14	8	5.11
L	Middle temporal gyrus	−54	−60	−2	6	5.46
R	Middle temporal gyrus	58	−56	−2	4	5.12
R	Middle temporal gyrus	46	−60	18	3	4.88
L	Fusiform gyrus	−26	−64	−10	8	5.54
R	Fusiform gyrus	26	−56	−10	4	5.14
Cluster 3: placebo > amisulpride						
R	Midbrain	10	−16	−14	3	5.10
R	Superior temporal gyrus	42	−12	−2	7	5.76
Cluster 6: amisulpride > placebo						
R	Superior frontal gyrus	2	56	30	4	5.00
R	Medial frontal gyrus	6	60	6	5	4.84
R	Anterior cingulate cortex	2	40	6	5	5.07
R	Anterior cingulate cortex	10	40	18	6	5.17
R	Superior frontal gyrus	30	60	18	5	4.95
L	Middle temporal gyrus	−46	−28	−6	4	5.90
R	Middle temporal gyrus	58	−16	−10	4	5.48
Cluster 6: placebo > amisulpride						
R	Entorhinal cortex	22	0	−38	6	5.52
R	Hippocampus	22	−36	6	4	5.13
L	Inferior temporal gyrus	−50	−52	−26	4	4.91
L	Precuneus	−6	−80	46	5	5.72

Anatomical labels, MNI coordinates (*x*, *y*, *z*), *z*-scores, and cluster size (number of voxels) for whole-brain connectivity of individual OFC subregions in the K6 parcellation contributing to the separation between groups, thresholded at $p < 0.05$, Bonferroni corrected ($z > 4.47$) and $k > 2$. L, Left; R, right.

with a marked reduction in the connectivity between the central OFC and the midbrain, suggesting that, relative to other parts of OFC, central OFC receives the strongest DA projections from the midbrain.

While null results should be interpreted with caution, the absence of significant DA-dependent changes in the K2 subdivision may imply that this subdivision scheme is not modulated by DA and that DA-dependent modulations occur only at a finer scale.

Subregions in the K2 parcellation are well in line with anatomical boundaries defined cytoarchitectonically and based on anatomical connections. The medial cluster corresponds to the agranular and dysgranular (i.e., nonisocortical) part of OFC and receives substantial input from the hippocampus and the amygdala. In contrast, the lateral-anterior cluster corresponds closely to the granular (i.e., isocortical) OFC and receives strong projections from the PFC, the insula, the temporal cortex, and the medial dorsal thalamus (Morecraft et al., 1992). This twofold parcellation scheme is also consistent with subdivisions based on intrinsic anatomical connections of the primate OFC (Carmichael and Price, 1994; Kahnt et al., 2012). However, although D2R blockade did not alter the outlines of the K2 subdivision, it did modulate the functional connectivity patterns of these subregions, suggesting that while the configuration of the coarse functional network was not affected by DA, the specific balance of connections within the network was changed.

The reconfiguration observed in the K6 parcellation is likely to be driven by a DA-dependent modulation of the connections between individual OFC voxels and remote brain regions. At the cellular level, amisulpride acts as an antagonist on D_2 and D_3 receptors, and reduces the postsynaptic effects of DA on neurons (Rosenzweig et al., 2002). In addition, amisulpride blocks presynaptic autoreceptors, effectively increasing the availability of DA in the synaptic cleft. Accordingly, any combination of presynaptic and postsynaptic receptor blockade will therefore increase the ratio of D_1 to D_2 receptor activation. By modulating the intrinsic firing properties of individual neurons, DA may change the strength of specific synapses and thereby the connectivity to other neurons, effectively altering the role of individual neurons in its larger circuit (Kloppenburg et al., 1999; Harris-Warrick and Johnson, 2010). Such changes are not necessarily binary switches (i.e., on–off) between connections, but could involve smooth transitions in the composition of interconnected networks. Interestingly, neuromodulator-induced changes in connectivity may be associated with different modes of operation responsible for different behaviors (Harris-Warrick and Marder, 1991; Weimann and Marder, 1994). The hard-wired anatomical connections between brain regions may therefore provide only the structure in which several possible functional networks, each associated with specific processing modes and behaviors, can be initialized depending on the current neuromodulatory environment (Brezina, 2010; Marder, 2012).

Our results show that connections between individual OFC subregions and higher-order sensory and multimodal association areas in the parietal and temporal lobes were dampened by D2R blockade. In contrast, connectivity between the OFC and the medial and superior PFC was upregulated by amisulpride. This suggests that DA activity on D2R switches the OFC between two distinct connectional configurations that may be associated with different processing modes. The first configuration, induced by high levels of D2R activity, is characterized by enhanced connectivity to higher sensory and associative areas, and may help sensory information to access the OFC. A second configuration, induced by low D2R activity, is characterized by enhanced short-range functional connections with the frontal lobes and may facilitate local information processing in the frontal cortex.

This proposal is in line with the effects of receptor-specific DA activity in a biophysically inspired dual-state model of DA in the PFC (Durstewitz et al., 2000; Seamans et al., 2001). Specifically, in this model, the ratio of D_1 and D_2 receptor activity modulates local GABAergic inhibition and thereby controls the balance between the stability and flexibility of PFC representations. Reduced D2R activity facilitates recurrent excitation in the network and stabilizes PFC representations, whereas enhanced D2R activity inhibits recurrent excitation and increases the flexibility of PFC representations (Seamans and Yang, 2004). Supporting this model, we have previously shown that D2R blockade enhances the decoding of reward information from OFC activity patterns, suggesting that corresponding network representations were strengthened (Kahnt et al., 2015).

Importantly, switches between the two OFC network configurations could be implemented solely by changes in local DA concentrations. Specifically, DA has a higher affinity for D_2 receptors than for D_1 receptors (Creese et al., 1983), and therefore low levels of DA may lead to stronger D_2 activity versus D_1 activity, whereas robust activity of D_1 receptors is achieved only with high levels of DA (Goto and Grace, 2005). Thus, bursts of DA, like those elicited by unexpected rewards or reward-predictive stimuli (Schultz et al., 1997; Schultz, 2016), may drive the OFC into a D_1-dominated state with enhanced connectivity to frontal brain regions and reduced connectivity to sensory areas, promoting local information processing and representational stability. Conversely, low levels of DA, like those observed when expected rewards are omitted (Bayer and Glimcher, 2005; Takahashi et al., 2009), may preferentially activate D_2 receptors, which may reduce connections to the PFC, enhance sensory input to the OFC, and facilitate reorientation, representational updating, and behavioral flexibility. Interestingly, a recent model of OFC functioning proposes that OFC contributes to goal-directed behavior by representing a cognitive map, or associative structure, for reinforcement learning (Wilson et al., 2014; Howard et al., 2015; Schuck et al., 2016; Wikenheiser and Schoenbaum, 2016). Our results indicate that DA may play a critical role in the updating of OFC state representations.

It is important to note that although amisulpride is one of the few relatively selective drugs affecting DA transmission, it also has high affinity for serotonin receptors 5-HT2B and 5-HT7. Accordingly, the effects observed here may not be the result of DA alone. However, insofar as serotonin and DA are both monoamines, we can conclude that our results are driven by monoaminergic neuromodulators. We also note that connectivity changes between the OFC and any other brain region may be caused indirectly through connectivity changes between this region and a third region whose connectivity to OFC is modulated by DA. Thus, OFC connectivity changes with individual areas need to be interpreted with caution because indirect modulations cannot be ruled out. Finally, in the current study, we examined the effects of D2R blockade on connectivity during rest. It is possible that OFC networks are differentially modulated during the performance of specific tasks. Functional connectivity between areas partially depends on task-dependent activity levels, which may result in different parcellation schemes. Future studies are needed to examine OFC network configurations as a function of different tasks.

In summary, here we have shown that D2R blockade changes the functional organization of the OFC. We speculate that midbrain DA may alter the connectional configuration of the OFC, leading to transitions between different operating modes that favor either sensory input or recurrent processing. Finally, the results obtained here for DA could exemplify a more general role of neuromodulators in altering the connec-

tivity patterns of brain regions. This change in connectivity may lead to the reconfiguration of specific functional circuits that may be associated with different modes of information processing and ultimately with distinct behaviors.

References

Bayer HM, Glimcher PW (2005) Midbrain dopamine neurons encode a quantitative reward prediction error signal. Neuron 47:129–141. CrossRef Medline

Brezina V (2010) Beyond the wiring diagram: signalling through complex neuromodulator networks. Philos Trans R Soc Lond B Biol Sci 365:2363–2374. CrossRef Medline

Carmichael ST, Price JL (1994) Architectonic subdivision of the orbital and medial prefrontal cortex in the macaque monkey. J Comp Neurol 346:366–402. CrossRef Medline

Carmichael ST, Price JL (1996) Connectional networks within the orbital and medial prefrontal cortex of macaque monkeys. J Comp Neurol 371:179–207. CrossRef Medline

Cavada C, Compañy T, Tejedor J, Cruz-Rizzolo RJ, Reinoso-Suárez F (2000) The anatomical connections of the macaque monkey orbitofrontal cortex. A review. Cereb Cortex 10:220–242. CrossRef Medline

Cetin T, Freudenberg F, Füchtemeie M, Koch M (2004) Dopamine in the orbitofrontal cortex regulates operant responding under a progressive ratio of reinforcement in rats. Neurosci Lett 370:114–117. CrossRef Medline

Clarke HF, Cardinal RN, Rygula R, Hong YT, Fryer TD, Sawiak SJ, Ferrari V, Cockcroft G, Aigbirhio FI, Robbins TW, Roberts AC (2014) Orbitofrontal dopamine depletion upregulates caudate dopamine and alters behavior via changes in reinforcement sensitivity. J Neurosci 34:7663–7676. CrossRef Medline

Cole DM, Beckmann CF, Oei NY, Both S, van Gerven JM, Rombouts SA (2013a) Differential and distributed effects of dopamine neuromodulations on resting-state network connectivity. Neuroimage 78:59–67. CrossRef Medline

Cole DM, Oei NY, Soeter RP, Both S, van Gerven JM, Rombouts SA, Beckmann CF (2013b) Dopamine-dependent architecture of cortico-subcortical network connectivity. Cereb Cortex 23:1509–1516. CrossRef Medline

Cools R (2016) The costs and benefits of brain dopamine for cognitive control. Wiley Interdiscip Rev Cogn Sci 7:317–329. CrossRef Medline

Creese I, Sibley DR, Hamblin MW, Leff SE (1983) The classification of dopamine receptors: relationship to radioligand binding. Annu Rev Neurosci 6:43–71. CrossRef Medline

Durstewitz D, Seamans JK, Sejnowski TJ (2000) Dopamine-mediated stabilization of delay-period activity in a network model of prefrontal cortex. J Neurophysiol 83:1733–1750. Medline

Eickhoff SB, Bzdok D, Laird AR, Roski C, Caspers S, Zilles K, Fox PT (2011) Co-activation patterns distinguish cortical modules, their connectivity and functional differentiation. Neuroimage 57:938–949. CrossRef Medline

Fox MD, Zhang D, Snyder AZ, Raichle ME (2009) The global signal and observed anticorrelated resting state brain networks. J Neurophysiol 101:3270–3283. CrossRef Medline

Goldman-Rakic PS, Lidow MS, Smiley JF, Williams MS (1992) The anatomy of dopamine in monkey and human prefrontal cortex. J Neural Transm Suppl 36:163–177. Medline

Goto Y, Grace AA (2005) Dopaminergic modulation of limbic and cortical drive of nucleus accumbens in goal-directed behavior. Nat Neurosci 8:805–812. CrossRef Medline

Harris-Warrick RM, Johnson BR (2010) Checks and balances in neuromodulation. Front Behav Neurosci 4:1–9. CrossRef Medline

Harris-Warrick RM, Marder E (1991) Modulation of neural networks for behavior. Annu Rev Neurosci 14:39–57. CrossRef Medline

Haufe S, Meinecke F, Görgen K, Dähne S, Haynes JD, Blankertz B, Bießmann F (2014) On the interpretation of weight vectors of linear models in multivariate neuroimaging. Neuroimage 87:96–110. CrossRef Medline

Honey GD, Suckling J, Zelaya F, Long C, Routledge C, Jackson S, Ng V, Fletcher PC, Williams SC, Brown J, Bullmore ET (2003) Dopaminergic drug effects on physiological connectivity in a human cortico-striato-thalamic system. Brain 126:1767–1781. CrossRef Medline

Howard JD, Gottfried JA, Tobler PN, Kahnt T (2015) Identity-specific coding of future rewards in the human orbitofrontal cortex. Proc Natl Acad Sci U S A 112:5195–5200. CrossRef Medline

Johansen-Berg H, Behrens TE, Robson MD, Drobnjak I, Rushworth MF, Brady JM, Smith SM, Higham DJ, Matthews PM (2004) Changes in connectivity profiles define functionally distinct regions in human medial frontal cortex. Proc Natl Acad Sci U S A 101:13335–13340. CrossRef Medline

Kahnt T, Chang LJ, Park SQ, Heinzle J, Haynes JD (2012) Connectivity-based parcellation of the human orbitofrontal cortex. J Neurosci 32:6240–6250. CrossRef Medline

Kahnt T, Weber SC, Haker H, Robbins TW, Tobler PN (2015) Dopamine D2-receptor blockade enhances decoding of prefrontal signals in humans. J Neurosci 35:4104–4111. CrossRef Medline

Kelly C, Uddin LQ, Shehzad Z, Margulies DS, Castellanos FX, Milham MP, Petrides M (2010) Broca's region: linking human brain functional connectivity data and non-human primate tracing anatomy studies. Eur J Neurosci 32:383–398. CrossRef Medline

Kloppenburg P, Levini RM, Harris-Warrick RM (1999) Dopamine modulates two potassium currents and inhibits the intrinsic firing properties of an identified motor neuron in a central pattern generator network. J Neurophysiol 81:29–38. Medline

Kringelbach ML, Rolls ET (2004) The functional neuroanatomy of the human orbitofrontal cortex: evidence from neuroimaging and neuropsychology. Prog Neurobiol 72:341–372. CrossRef Medline

Mackey S, Petrides M (2010) Quantitative demonstration of comparable architectonic areas within the ventromedial and lateral orbital frontal cortex in the human and the macaque monkey brains. Eur J Neurosci 32:1940–1950. CrossRef Medline

Marder E (2012) Neuromodulation of neuronal circuits: back to the future. Neuron 76:1–11. CrossRef Medline

Meilă M (2007) Comparing clusterings—an information based distance. J Multivar Anal 98:873–895. CrossRef

Miller EK, Cohen JD (2001) An integrative theory of prefrontal cortex function. Annu Rev Neurosci 24:167–202. CrossRef Medline

Morecraft RJ, Geula C, Mesulam MM (1992) Cytoarchitecture and neural afferents of orbitofrontal cortex in the brain of the monkey. J Comp Neurol 323:341–358. CrossRef Medline

Nagano-Saito A, Leyton M, Monchi O, Goldberg YK, He Y, Dagher A (2008) Dopamine depletion impairs frontostriatal functional connectivity during a set-shifting task. J Neurosci 28:3697–3706. CrossRef Medline

Ongür D, Price JL (2000) The organization of networks within the orbital and medial prefrontal cortex of rats, monkeys and humans. Cereb Cortex 10:206–219. CrossRef Medline

Padoa-Schioppa C (2011) Neurobiology of economic choice: a good-based model. Annu Rev Neurosci 34:333–359. CrossRef Medline

Rosenzweig P, Canal M, Patat A, Bergougnan L, Zieleniuk I, Bianchetti G (2002) A review of the pharmacokinetics, tolerability and pharmacodynamics of amisulpride in healthy volunteers. Hum Psychopharmacol 17:1–13. CrossRef Medline

Rudebeck PH, Murray EA (2014) The orbitofrontal oracle: cortical mechanisms for the prediction and evaluation of specific behavioral outcomes. Neuron 84:1143–1156. CrossRef Medline

Rushworth MF, Kolling N, Sallet J, Mars RB (2012) Valuation and decision-making in frontal cortex: one or many serial or parallel systems? Curr Opin Neurobiol 22:946–955. CrossRef Medline

Schuck NW, Cai MB, Wilson RC, Niv Y (2016) Human orbitofrontal cortex represents a cognitive map of state space. Neuron 91:1402–1412. CrossRef Medline

Schultz W (2016) Dopamine reward prediction-error signalling: a two-component response. Nat Rev Neurosci 17:183–195. CrossRef Medline

Schultz W, Dayan P, Montague PR (1997) A neural substrate of prediction and reward. Science 275:1593–1599. CrossRef Medline

Seamans JK, Yang CR (2004) The principal features and mechanisms of dopamine modulation in the prefrontal cortex. Prog Neurobiol 74:1–58. CrossRef Medline

Seamans JK, Gorelova N, Durstewitz D, Yang CR (2001) Bidirectional dopamine modulation of GABAergic inhibition in prefrontal cortical pyramidal neurons. J Neurosci 21:3628–3638. Medline

Sescousse G, Redouté J, Dreher JC (2010) The architecture of reward value coding in the human orbitofrontal cortex. J Neurosci 30:13095–13104. CrossRef Medline

Stalnaker TA, Cooch NK, Schoenbaum G (2015) What the orbitofrontal cortex does not do. Nat Neurosci 18:620–627. CrossRef Medline

Swanson LW (1982) The projections of the ventral tegmental area and ad-

jacent regions: a combined fluorescent retrograde tracer and immunofluorescence study in the rat. Brain Res Bull 9:321–353. CrossRef Medline

Takahashi YK, Roesch MR, Stalnaker TA, Haney RZ, Calu DJ, Taylor AR, Burke KA, Schoenbaum G (2009) The orbitofrontal cortex and ventral tegmental area are necessary for learning from unexpected outcomes. Neuron 62:269–280. CrossRef Medline

Van Dijk KR, Hedden T, Venkataraman A, Evans KC, Lazar SW, Buckner RL (2010) Intrinsic functional connectivity as a tool for human connectomics: theory, properties, and optimization. J Neurophysiol 103:297–321. CrossRef Medline

Walker SC, Robbins TW, Roberts AC (2009) Differential contributions of dopamine and serotonin to orbitofrontal cortex function in the marmoset. Cereb Cortex 19:889–898. CrossRef Medline

Weimann JM, Marder E (1994) Switching neurons are integral members of multiple oscillatory networks. Curr Biol 4:896–902. CrossRef Medline

Wikenheiser AM, Schoenbaum G (2016) Over the river, through the woods: cognitive maps in the hippocampus and orbitofrontal cortex. Nat Rev Neurosci 17:513–523. CrossRef Medline

Wilson RC, Takahashi YK, Schoenbaum G, Niv Y (2014) Orbitofrontal cortex as a cognitive map of task space. Neuron 81:267–279. CrossRef Medline

Winstanley CA, Zeeb FD, Bedard A, Fu K, Lai B, Steele C, Wong AC (2010) Dopaminergic modulation of the orbitofrontal cortex affects attention, motivation and impulsive responding in rats performing the five-choice serial reaction time task. Behav Brain Res 210:263–272. CrossRef Medline

Zald DH, Rauch SL (2008) The orbitofrontal cortex. Oxford/New York: Oxford UP.

Zald DH, McHugo M, Ray KL, Glahn DC, Eickhoff SB, Laird AR (2014) Meta-analytic connectivity modeling reveals differential functional connectivity of the medial and lateral orbitofrontal cortex. Cereb Cortex 24:232–248. CrossRef Medline